(2)

MTL TR 89-97

AD-A217 262

EVALUATION OF 2090-T8E48 ALUMINUM-LITHIUM PLATES

ERNEST S. C. CHIN
MATERIALS PRODUCIBILITY BRANCH

MARIETTA R. CAPPUCCI and ROBERT M. HUIE
METALS RESEARCH BRANCH

ROBERT E. PASTERNAK
MATERIALS TEST AND EVALUATION BRANCH

November 1989

Approved for public release; distribution unlimited.

US ARMY
LABORATORY COMMAND
MATERIALS TECHNOLOGY LABORATORY

U.S. ARMY MATERIALS TECHNOLOGY LABORATORY
Watertown, Massachusetts 02172-0001

UNCLASSIFIED

SECURITY CLASSIFICATION OF THIS PAGE (When Data Entered)

REPORT DOCUMENTATION PAGE		READ INSTRUCTIONS BEFORE COMPLETING FORM
1. REPORT NUMBER MTL TR 89-97	2. GOVT ACCESSION NO.	3. RECIPIENT'S CATALOG NUMBER
4. TITLE (and Subtitle) EVALUATION OF 2090-T8E48 ALUMINUM-LITHIUM PLATES		5. TYPE OF REPORT & PERIOD COVERED Final Report 6. PERFORMING ORG. REPORT NUMBER
7. AUTHOR(s) Ernest S. C. Chin, Marietta R. Cappucci, Robert M. Huie, and Robert E. Pasternak		8. CONTRACT OR GRANT NUMBER(s)
9. PERFORMING ORGANIZATION NAME AND ADDRESS U.S. Army Materials Technology Laboratory Watertown, Massachusetts 02172-0001 SLCMT-MEM		10. PROGRAM ELEMENT, PROJECT, TASK AREA & WORK UNIT NUMBERS D/A Project: 1L162105.AH84
11. CONTROLLING OFFICE NAME AND ADDRESS U.S. Army Laboratory Command 2800 Powder Mill Road Adelphi, Maryland 20783-1145		12. REPORT DATE November 1989 13. NUMBER OF PAGES 19
14. MONITORING AGENCY NAME & ADDRESS (if different from Controlling Office)		15. SECURITY CLASS. (of this report) Unclassified 15a. DECLASSIFICATION/DOWNGRADING SCHEDULE

16. DISTRIBUTION STATEMENT (of this Report)

Approved for public release; distribution unlimited.

17. DISTRIBUTION STATEMENT (of the abstract entered in Block 20, if different from Report)

18. SUPPLEMENTARY NOTES

19. KEY WORDS (Continue on reverse side if necessary and identify by block number)

Aluminum alloys	Toughness
Lithium alloys	Ballistics
Tensile strength	Corrosion

20. ABSTRACT (Continue on reverse side if necessary and identify by block number)

(SEE REVERSE SIDE)

DD FORM 1 JAN 73 1473 EDITION OF 1 NOV 65 IS OBSOLETE

UNCLASSIFIED

SECURITY CLASSIFICATION OF THIS PAGE (When Data Entered)

Block No. 20

ABSTRACT

A 1.5-inch-thick 2090-T8E48 aluminum-lithium (Al-Li) alloy plate was evaluated in conjunction with the Navy Cooperative Test Program. Mechanical characterization included testing of tensile specimens in the longitudinal, transverse, and short direction, and testing of compact tension/slow bend specimens covering the L-T, T-L, L-S, S-L, S-T, and T-S directions. In addition, ballistic tolerance against caliber .30 armor piercing projectile and 20-mm fragment simulated projectile was determined. Corrosion and stress corrosion studies were made in accordance with ASTM standards. Microstructural characterization was performed through optical metallography and transmission electron microscopy. Consolidation and discussion of all the results in comparison with previously evaluated 0.5-inch-thick X2090-T8 is presented. (AU)

CONTENTS

Page

INTRODUCTION 1

EXPERIMENTAL PROCEDURES

- Mechanical Testing 2
- Ballistic Testing 2
- Corrosion and Stress Corrosion Evaluation 2
- Microstructural Analysis 3

RESULTS AND DISCUSSION

- Tensile and Fracture Toughness Testing 3
- Corrosion Behavior 8
- Microstructural Analysis 10

CONCLUSIONS 15

INTRODUCTION

The first commercial aluminum-lithium (Al-Li) alloy was introduced in the 1950's and was designated as 2020 by the Aluminum Company of America (ALCOA). The development of 2020 was primarily tailored for airframe applications.[1] Due to difficulties in fabrication and the low fracture toughness properties exhibited in this alloy, 2020 was withdrawn from production in the late 1960's. Research studies on Al-Li alloys in the Soviet Union continued, which led to the development of a weldable 1420 Al-Li alloy.[2] Due to an increasing demand for stiffer and lighter aluminum alloys in the 1970's for aerospace applications, interest in Al-Li alloys was renewed in the United States. A number of commercially available Al-Li alloys are now available.

In the early 1980's, the U.S. Army Materials Technology Laboratory (MTL) participated in the Navy's Cooperative Test Program on Al-Li alloys to establish a material property data base. The purpose of this task was to keep abreast of new developments in Al-Li alloys, as well as to identify potential Army applications. The first group of materials evaluated consisted of 0.5-inch-thick X2090-T8E41 plates and X2090-T8 "T" shape extrusions. Results from that study were disappointing.[3] Poor fracture toughness at room and at elevated temperature was exhibited by the as-received X2090-T8E41. Furthermore, the ballistic penetration (V_{50}) results showed X2090-T8E41 to be only comparable to 7039-T64 at the same areal density against caliber .30 armor piercing (cal. .30 AP M2) round and against caliber .50 fragment simulated projectiles (cal. .50 FSP). Severe spalling and delamination observed in the testing precluded X2090 from further consideration as an armor candidate. The poor fracture toughness and ballistic performance in X2090-T8E41 were due to excess iron-rich precipitates aligned along primary grain boundaries.

Since the study made on the X2090-T8E41, ALCOA reported an improvement in processing of X2090 that resulted in a lower iron limit. Concurrently, X2090 was designated as commercial 2090 Al and thicker plates up to 1.5 inches became available. Recent studies at the ALCOA Technical Center also reported good welding characteristics[4] and good exposure resistance[5] in 2090-T8. All indications pointed toward readiness of 2090-T8 for a variety of Army applications.

In July 1988, MTL received 1.5-inch-thick plates of 2090-T8E48 Al-Li from ALCOA as the second phase of the Navy's Cooperative Test Program. The purpose of this report is to document mechanical properties, ballistic performance, corrosion and stress corrosion behavior, and microstructural characteristics of the as-received 1.5-inch-thick 2090-T8E48 plates.

1. BALMUTH, E. S., and SCHMIDT, R. in Aluminum-Lithium Alloys. T. H. Sanders and E. A. Starke, ed., TMS-AIME, New York, 1989, p. 69.
2. FRIDLYANDER, I. N., and GABIDULLIN, S. M. *New Light Alloys of Aluminum Lithium and Magnesium*. Met. Sci. Heat Treat. Met., no. 3, translated from Metaloved. Term. Obrab. Met., no. 3, March 1968, p. 50-52.
3. BUSCEMI, C. S., and CHIN, E. *Characterization of X2090 Al-Li Alloy*. U.S. Army Materials Technology Laboratory, MTL TR 88-26, September 1988.
4. MARTUKANITZ, R. P., NATALIE, C. A., and KNOEFEL, J. O. *The Weldability of 2090 (An Al-Li-Cu Alloy)*. Journal of Metals, v. 39, no. 11, November 1987, p. 38-42.
5. MALCOLM, R. C., CORDIER, F. J., and BUCCI, R. J. *The Effects of Various Thermal Conditions on the Tensile Properties of Aluminum Alloy 2090-T8E41 Plate (0.5-Inch Thick)*. Alloy Technology Division Report Number 56-86-AH429, ALCOA, October 23, 1986.

EXPERIMENTAL PROCEDURES

Mechanical Testing

Mechanical characterization of the as-received 2090-T8E48 plate included determination of tensile and fracture toughness properties. Ultimate tensile strengths (UTS), yield strengths, elongation, and modulus were obtained from testing of 0.505-inch- and 0.113-inch-diameter threaded round tensile specimens. Due to the thickness constraint, only subsize (0.113 inch diameter) tensile specimens were tested in the through thickness (short) direction. Subsize tensile specimens (0.113 inch diameter) along with standard (0.505 inch diameter) specimens were tested in the longitudinal and transverse directions to determine possible size effects to gauge tensile data in the short direction. Tensile testing was performed in accordance with ASTM B 557, Tension Testing Wrought and Cast Aluminum and Magnesium Alloy Products. Fracture toughness testing of 2090-T8E48 Al-Li plate was conducted according to ASTM E 399, Standard Test Method for Plane-Strain Fracture Toughness of Metallic Materials. Both bend and compact specimens were tested in a variety of sizes and orientations. The compact specimens included the following thicknesses and orientations: 1.5 inch thick (L-T, T-L), 0.75 inch thick (L-T, T-L), and 0.5 inch thick (L-T, T-L, S-L, L-S, T-S, S-T). All the bend specimens were 0.505 inch thick (L-T, T-L, T-S, L-S). Slow bend specimens were tested for the purpose of direct comparison with the X2090-T8E41 fracture toughness data of the same thickness and test specimen type.

Ballistic Testing

Ballistic tolerance of the as-received 2090-T8E48 plates was established through determination of V_{50} against cal. .30 AP M2 and 20-mm fragment simulating projectiles (FSP). The ballistic limit V_{50} is defined as the velocity at which a specific projectile impacted at a specified obliquity on a particular material and thickness has a 50% probability of penetration. The test procedure used in obtaining V_{50} at MTL is in accordance with U.S. Army Test and Evaluation Command Test Operation Procedure 2-2-710 DRSTE-RP-702-101 (AD No. A137873). The 2090-T8E48 Al-Li ballistic target plates were tested in the as-received 1.5-inch-thick condition.

Corrosion and Stress Corrosion Evaluation

The objective of this evaluation was to determine the susceptibility of Al alloy 2090-T8E48 to SCC in 3.5% NaCl solution as a function of specimen orientation. The selfstressed, precracked, double-cantilever-beam (DCB) specimen was selected for determination of K_{Iscc}, the stress intensity threshold below which no crack growth occurs.

The DCB specimen which is particularly suited for testing in the short transverse direction (S-L, S-T) was bolt loaded and mechanically precracked. Upon exposure to the NaCl solution, stress corrosion crack growth occurred and the propagation of the crack was measured on two surfaces of the specimen. As the crack length increased, the crack tip intensity decreased, the crack growth rate decreased, and the crack arrested or reached a reasonably low crack growth rate of 10 to 6 in./hr and a corresponding stress intensity designated as K_{Iscc}. Finally, the specimen was broken open and the fracture surfaces were examined. Three distinct areas were revealed: mechanical precrack; SCC crack growth; and, finally, mechanical fracture after test. The DCB specimen shown in Figure 1 was tested in the T-L, S-T, and S-L orientations.

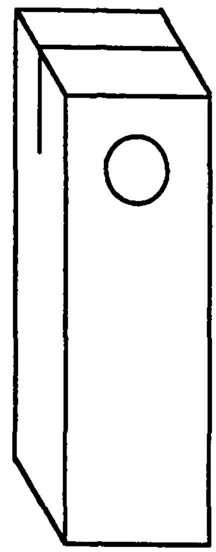

Figure 1. Double cantilever beam specimen.

Microstructural Analysis

Microstructural characterization was performed using both light metallography and electron microscopy. Metallographic specimens were sectioned from various orientations of the as-received plate. The microstructures were determined from specimens polished and etched using Keller's reagent. Transmission electron microscopy (TEM) specimens in the form of 3-mm discs were electropolished in a twin-jet electropolishing unit using a 3:1 methanol:nitric acid electrolyte cooled to -20°C with a potential difference of 10 V. TEM thin foils were examined on a Phillips EM 400 T electron microscope. Fractographic analysis of both 0.505-inch and 0.113-inch tensile specimens was performed on an AMRAY 1645 scanning electron microscope (SEM).

RESULTS AND DISCUSSION

Tensile and Fracture Toughness Testing

Longitudinal, transverse, and through thickness (short) tensile properties of 2090-T8E48 are shown in Tables 1, 2, and 3, respectively. Tensile data of 2090-T8E48 provided by ALCOA, of X2090-T8E41,[3] of 2519-T87 Al, and of 7039-T67 Al[6] are also presented for comparison. Evaluation of tensile data showed slight improvement over the previously tested X2090-T8E41. Ultimate tensile strength and yield strength were better than the values reported for 2519-T87 and 7039-T64 armor alloys. Discrepancies were observed comparing tensile properties between the 0.505-inch and the 0.113-inch gauge diameter specimens. Size and strain rate effects appeared to have influenced the tensile properties between the two types of specimens. This phenomena will be further discussed under the Microstructural Analysis Section. All the 0.505-inch tensile results corresponded with data provided by ALCOA from limited testing.

6. DeLUCA, E., and ANCTIL, A. A. *Laminate Armor for Light Combat Vehicles.* U.S. Army Materials Technology Laboratory, MTL TR 86-14, April 1986.

Table 1. LONGITUDINAL TENSILE PROPERTIES

Material	Number of Tests	Gauge Diameter (in.)	Ultimate Tensile Strength (ksi)	0.2% Yield Strength (ksi)	Elongation (%)
2090-T8E48	5	0.113	77.0 (75.0-79.0)*	71.0 (69.0-73.0)	4.1 (2.7-5.5)
	6	0.505	85.0 (84.0-85.0)	81.0 (81.0-82.0)	8.5 (7.6-10.1)
ALCOA's Data on 2090-T8E48	4	—	85.0 (85.0-86.0)	81.0 (81.0-82.0)	6.8 (6.0-7.0)
X2090-T8E41	3	0.505	82.0 (81.0-86.0)	78.0 (76.0-83.0)	5.6 (5.3-5.9)
2519-T87	—	—	67.0	61.0	12.0
7039-T64	—	—	66.0	58.0	13.0

*Numbers in parentheses represent spread

Table 2. TRANSVERSE TENSILE PROPERTIES

Material	Number of Tests	Gauge Diameter (in.)	Ultimate Tensile Strength (ksi)	0.2% Yield Strength (ksi)	Elongation (%)
2090-T8E48	8	0.113	77.0 (75.0-79.0)*	71.0 (64.0-77.0)	8.9 (3.8-13.5)
	6	0.505	84.0 (83.0-85.0)	79.0 (79.0-81.0)	7.0 (6.0-9.0)
ALCOA's Data on 2090-T8E48	4	—	84.0 (84.0-85.0)	79.0 (78.0-80.0)	4.5 (4.0-5.0)
X2090-T8E41	3	0.505	82.0 (81.0-84.0)	76.0 (75.0-78.0)	8.5 (7.8-8.9)
2519-T87	—	—	68.0	59.0	12.0
7039-T64	—	—	60.0	51.0	13.6

*Numbers in parentheses represent spread

Table 3. THROUGH THICKNESS TENSILE PROPERTIES

Material	Number of Tests	Gauge Diameter (in.)	Ultimate Tensile Strength (ksi)	0.2% Yield Strength (ksi)	Elongation (%)
2090-T8E48	18	0.113	71.2 (67.0-75.0)*	63.8 (61.0-65.0)	—
ALCOA's Data on 2090-T8E48	10	—	70.0 (66.0-74.0)	64.0 (63.0-66.0)	1.1 (0.5-2.0)

*Numbers in parentheses represent spread

Through thickness tensile properties are summarized in Table 3. Again, the properties shown confirmed results from ALCOA. Since a size effect was observed between the 0.505-inch- and 0.113-inch-diameter specimens in the longitudinal and transverse directions, better properties are anticipated with 0.505-inch-diameter specimens in the through thickness direction.

In general, 2090-T8E48 performs better in tensile testing than 2519-T87 and 7039-T64 aluminum armor alloys. Evaluation of tensile data indicates better ballistic resistance with 2090-T8E48 than 2519-T87 and 7039-T67.

Due to the texturing in the base material, precracking the fracture toughness specimens appeared to be a major difficulty. In an effort to detect crack initiation without having to constantly monitor the crack, the 1.5-inch-thick compact specimens were fitted with crack detection gauges. The gauges were applied using either a cyanoacrylate or epoxy adhesive. The output from the gauge circuit was monitored by a computerized data acquisition system. The monitoring system was also used to start/stop the function generator which controlled the load applied by the test machine. It was hoped that crack initiation would be detected by the computer and the test stopped before unstable crack growth took place. In theory, and during simulations, the system performed as expected. In practice, however, it was never possible to make the crack in the specimen propagate through the adhesive and break the grid of the gauge, thereby stopping the test. Although this method of monitoring crack growth proved unsuccessful, it did provide us with the confidence that a crack could be initiated in this material and grown in a controlled manner.

Precracking loads for the remaining specimens were kept low so that the maximum stress intensity factor did not exceed approximately 30% of the estimate K_Q (a conditional K_{Ic}). The low loads provided slow crack growth and allowed the machine to be set to run a fixed number of cycles with confidence that unstable crack growth would not occur. In addition, if the crack should reach the proper length ($0.45<a/W<0.55$) during cycling, the stress intensity for final crack growth would be within the limit specified in ASTM E 399.

In spite of the polished surfaces, crack monitoring and surface crack measurement remained a problem. Surface cracks were extremely fine and difficult to measure. The texturing within the specimen seems to have a pronounced effect on fatigue crack growth. Crack front profiles often had a scalloped appearance as different portions of the crack front grew at different rates. In one extreme case, a crack extended from one face across only about 90% of the notch with the internal end of the crack growing as if it were at a free edge.

The direction of texturing in certain specimens seemed to be the dominant force in determining the direction of crack propagation. In some cases, crack branching and crack propagation at 90 degrees to the desired direction were noted. While precracks could be generated in all the bend bars by using low loads, wh^n the specimens were tested to determine the value of K_Q, the cracks in the specimens for T-L, L-S, and T-S orientations propagated at 90 degrees to the precrack and made th ts invalid.

Summaries of the fracture toughness testing are presented in Tables 4, 5, and 6. Toughness properties of 2519-T87 and 7039-T67 from a previous MTL study[6] along with ALCOA's data of the same material are also presented for comparison. As anticipated, the best fracture toughness properties were exhibited by specimens tested in the L-T direction. The K_Q and valid K_{Ic} values were comparable to ALCOA's data as well as what was obtained with X2090-T8E41 from the previous investigation. Expected improvement was not well defined. The toughness properties were lower than those for 7039-T64 but comparable to 2519-T87 in the L-T direction.

Table 4. FRACTURE TOUGHNESS PROPERTIES/L-T DIRECTION

Material	Spec. Type*	No. of Tests	Thickness (in.)	K_Q (ksi$\sqrt{in.}$)	K_{Ic} (ksi$\sqrt{in.}$)
2090-T8E48	CT	4	1.40	31.3 (24.0-32.0)†	24.4
	CT	4	0.75	30.6 (28.0-32.0)	—
	CT	3	0.50	26.2 (22.0-31.0)	30.5
	B	4	0.50	30.7 (26.0-34.0)	—
ALCOA's Data on 2090-T8E48	—	2	—	34.0 (33.0-35.0)	—
X2090-T8E41	B	3	0.50	30.2 (29.0-32.0)	—
2519-T87	CT	7	—	—	27.2
7039-T64	CT	6	—	—	40.7

*CT = compact tension, B = slow bend
†Numbers in parentheses represent spread

Table 5. FRACTURE TOUGHNESS PROPERTIES/T-L DIRECTION

Material	Spec. Type*	No. of Tests	Thickness (in.)	K_Q (ksi$\sqrt{in.}$)	K_{Ic} (ksi$\sqrt{in.}$)
2090-T8E48	CT	4	1.43	24.5 (23.0-25.0)†	24.4 (23.0-25.0)
	CT	3	0.75	22.5 (21.0-23.0)	23.2 (23.1-23.3)
	CT	4	0.50	23.2 (22.0-24.0)	21.9
ALCOA's Data on 2090-T8E48	—	2	—	—	27.0 (24.0-30.0)
X2090-T8E41	B	3	0.50	29.7 (27.0-32.0)	—
2519-T87	CT	8	—	—	24.2
7039-T64	CT	6	—	—	35.6

*CT = compact tension, B = slow bend
†Numbers in parentheses represent spread

Table 6. FRACTURE TOUGHNESS PROPERTIES/THROUGH THICKNESS (S) DIRECTIONS

Material	Direction	Spec. Type*	No. of Tests	Thickness (in.)	K_Q (ksi$\sqrt{in.}$)	K_{Ic} (ksi$\sqrt{in.}$)
2090-T8E48	S-T	CT	3	0.5	8.6 (7.5-9.4)†	7.5
ALCOA's Data on 2090-T8E48	S-T	—	1	—	7.0-8.0	—
2090-T8E48	S-L	CT	1	0.5	—	16.9
2519-T87	S-L	CT	9	—	—	21.2
2090-T8E48	L-S	CT	4	0.5	18.2 (16.0-20.0)	—
2519-T87	L-S	CT	12	—	—	34.8
2090-T8E48	T-S	CT	3	0.5	13.7 (8.0-19.0)	16.7 (15.0-19.0)

*CT = compact tension, B = slow bend
†Numbers in parentheses represent spread

In the T-L direction, the valid K_{Ic} values obtained from MTL's testing were slightly lower than what was reported by ALCOA. Direct comparison with X2090-T8E41 cannot be made since 0.5-inch-thick bend specimens in the T-L direction were not available. The toughness properties of 2090-T8E48 in the T-L direction had lower value than 7039-T64 but higher than 2519-T87.

Fracture toughness values from the S-T, S-L, L-S, and T-S directions were all low for an aluminum alloy. These low values reflected the highly anisotropic nature of the plate due to texturing from the rolling process. This observation would also account for the difficulties in precracking the compact tension and slow bend specimens.

Ballistic results of 2090-T8E48, 2519-T87, and 7039-T64 against cal. .30 AP M2 at 30° obliquity and against 20-mm FSP at 0° obliquity are summarized in Table 7. As shown in Table 7, V_{50} values were better than 2519-T87 and 7039-T67 against the cal. .30 AP M2, but were lower against the 20-mm FSP at the same areal density. Postmortem examination of the 2090-T8E48 target plate showed severe spalling and delamination (see Figure 2).

Table 7. 2090-T8E48 BALLISTIC PROPERTIES

Material	Areal Density (psf)	Projectile	Obliquity (degree)	V_{50} (ft/sec)
2090-T8E48	20	Cal. .30 AP M2	30	3403
2519-T87	20	Cal. .30 AP M2	30	3200
7039-T67	20	Cal. .30 AP M2	30	2950
2090-T8E48	20	20-mm FSP	0	2368
2519-T87	20	20-mm FSP	0	2930
7039-T67	20	20-mm FSP	0	2450

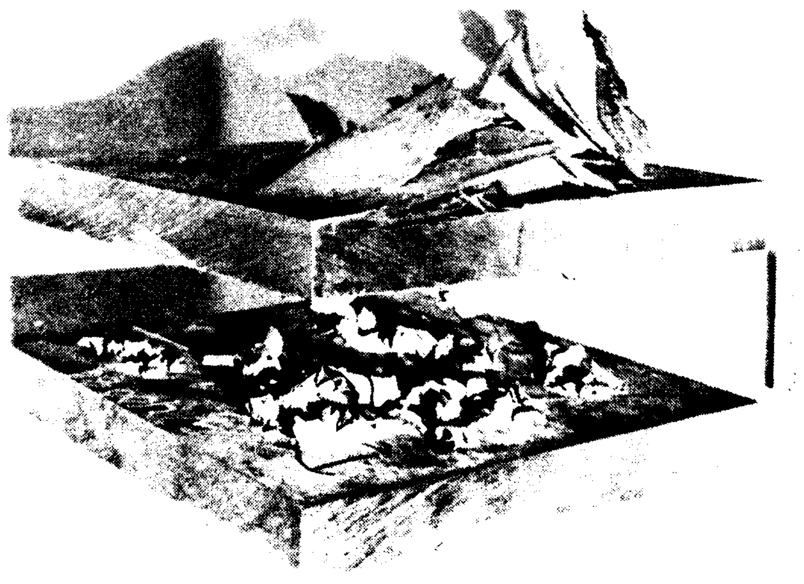

Figure 2. 2090-T8E48 ballistic target plates.

Corrosion Behavior

The DCB specimens couldn't be loaded by mechanical pop-in. The L-T specimens were very susceptible to precracking in a direction normal to the centerline and, therefore, could not be tested. The T-L specimens also exhibited this tendency to a lesser extent. As a consequence, the T-L, S-T, and S-L specimens were mechanically fatigue precracked prior to bolt loading. The K_{Iscc} data obtained from the DCB test is given in Table 8. A gelatinous compound formed on the surface of the DCB specimens (see Figure 3) especially at the crack tip. This gel, which is comprised of aluminum hydroxide $Al(OH)_3$ and lithium hydroxide (LiOH), was also observed at various locations on the surface of the specimen wherever corrosion (pitting, cracking) occurred. Upon air drying, the gel became a white, fine powder which was easily removed from the specimen by scraping. However, in the gel form, this substance adhered very strongly to the surface of the specimen and also in the cracks and pits and was extremely difficult to remove. The gel was not removed from the specimen each time the crack length was measured since it was a corrosion product. At the end of the SCC test, the gel was removed from the surface and the surface was polished with 400-grit silicon carbide paper to more accurately determine the final length of the crack. A large amount of pitting was observed throughout the specimen and especially along the high stress areas near the crack tip (see Figure 3).

Table 8. STRESS CORROSION DATA ON 2090-T8E48 PLATE

Orientation	K_{Iscc} (ksi$\sqrt{in.}$)
T-L	12-13
S-T	5-6
S-L	7

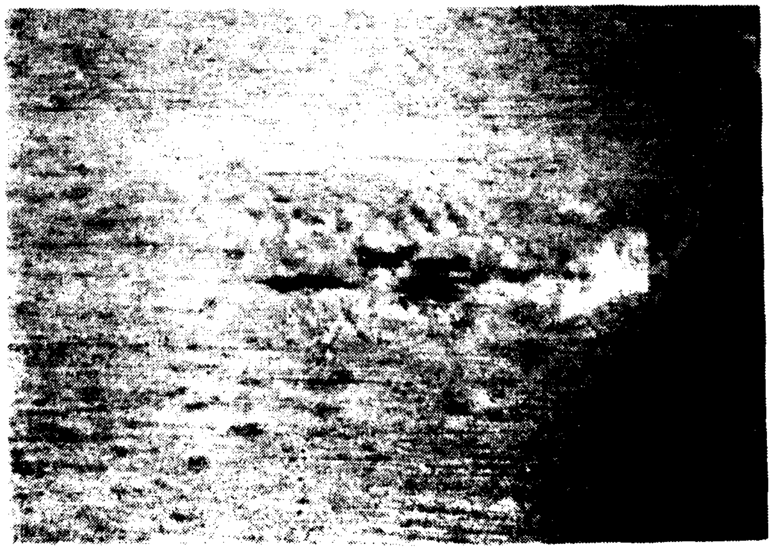

Figure 3. Photo of gel formation on pit surface of specimen T-L at 25X.

Finally, the specimens were loaded to fracture and the fracture surfaces examined for evidence of SCC. SEM examination of the slow crack growth area showed an intergranular fracture mode (see Figure 4). Intergranular SCC of Al alloys generally involves electrochemical reactions between the matrix, precipitates, and precipitate-free zones. Microstructural analysis of the 2090-T8E48 has shown the presence of coarse grain boundary precipitates. One of the most likely precipitates is T_2 (Al_6CuLi_3). Among the fine precipitates present is T_1 (Al_2CuLi). Because of the active nature of lithium, T_1 is probably an anodic phase relative to the matrix, and the grain boundary region should dissolve preferentially, leading to SCC susceptibility. The T_2 precipitate is probably even more anodic than T_1 because of more lithium and less Cu. The corrosion observed on the surface appeared to mask an intergranular attack along the crack surface. EDS analysis of this surface primarily identified Al with a relatively large amount of chloride and a trace amount of copper.

Figure 4. SEM micrograph of intergranular cracking in the SCC region of S-T at 1500X.

As expected, the S-L and S-T orientations of the alloy were the most susceptible to SCC (see Table 8). The K_{Iscc} values ranged from 5 to 7 ksi$\sqrt{in.}$. Thus, the 2090-T8E48 alloy is not as SCC-resistant as Al 5083 which has a K_{Iscc} of between 10 to 20 ksi$\sqrt{in.}$. The T-L orientation (normal to the rolling direction) exhibited higher K_{Iscc} values of 12 to 13 ksi$\sqrt{in.}$. The pitting resistance, however, was very poor. Pitting occurred at high stress areas adjacent to the crack tip and along the crack edges. Gel formation, which was present whenever corrosion occurred, appeared to slow the corrosion process by impeding the penetration of H_2O and Cl^- and mitigating the propensity for H^+ buildup and a more acidic crack tip chemistry. The crack tip blunting observed appeared to be due to the pitting that occurred in the area of the crack tip. The resultant increase in the area of the crack tip decreased the stress intensity and decreased the stress per unit area. Thus, the rate of crack propagation was retarded causing more pitting than crack growth to occur. The magnitude of pitting around the crack tip further relieved the stresses in that area, causing the crack to arrest.

In brief summary, the 2090-T8E48 alloy is highly susceptible to SCC in the S-L and S-T orientations. The alloy is not as susceptible in the T-L orientation. SEM examination showed an intergranular SCC failure mode. The severe pitting apparent was associated with the formation of an adherent gel.

Microstructural Analysis

Light microscopy revealed that the 2090-T8E48 plate had an extremely directional microstructure with elongated grains. A small degree of recrystallization occurred, accompanied by the formation of low-angle subgrain boundaries. Large precipitates outlined grain boundaries, and EDS indicated that several precipitates were Fe/Cu-rich. These coarse grain boundary precipitates were most likely the Al_7Cu_2Fe constituent phase and the T_2 (Al_6CuLi_3) identified in previous studies.[7-9] Isolated precipitation was also visible along subgrain boundaries, but not to as great an extent as along grain boundaries (see Figure 5). This 2090-T8E48 plate was fabricated with a reduced impurity content over that of the originally studied X2090-T8E41 plate.[3] As a result, grain boundaries in the 2090-T8E48 plate were not as heavily delineated by precipitates as were grain boundaries in the less clean X2090-T8E41 plate and extrusion examined by Chin and Buscemi.[3] A mean free path for precipitates along grain boundaries in the 2090-T8E48 plate was measured to be 4.3 μm.

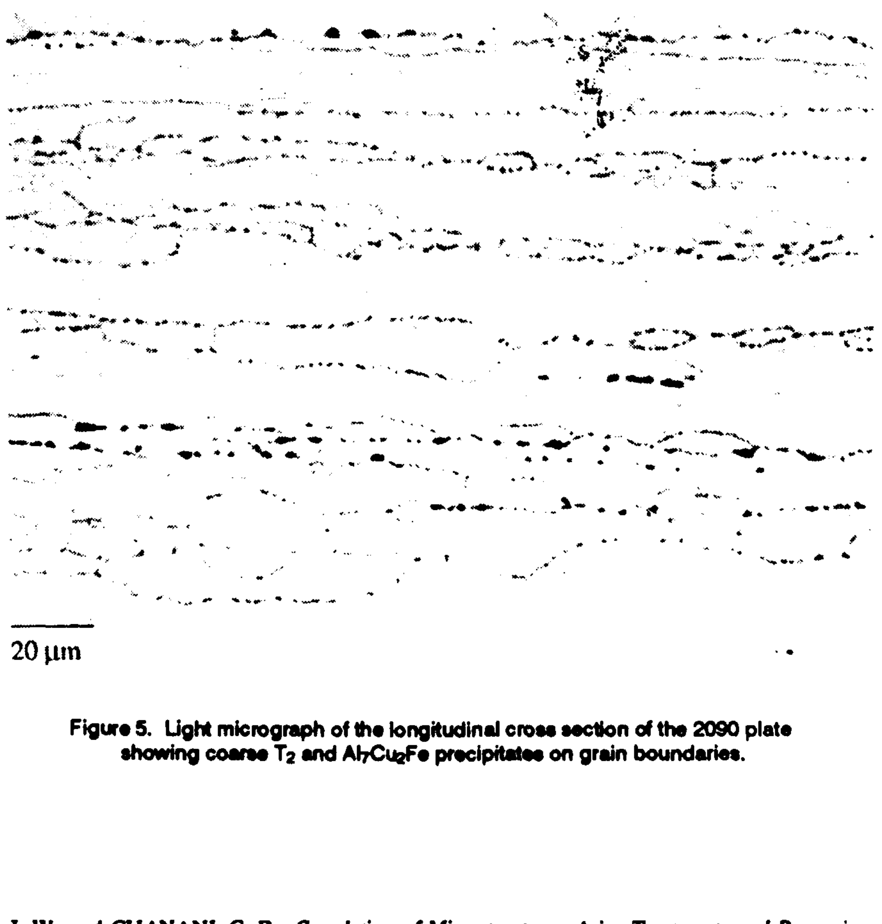

Figure 5. Light micrograph of the longitudinal cross section of the 2090 plate showing coarse T_2 and Al_7Cu_2Fe precipitates on grain boundaries.

7. KAR, R. J., BOHLEN, J. W., and CHANANI, G. R. *Correlation of Microstructures, Aging Treatments and Properties of Al-Li-Cu-Mg-Zr I/M and P/M Alloys.* Northrup Corporation IR&D Report.
8. GYSLER, A., CROOKS, R., and STARKE, Jr., E. A. *A Comparison of Microstructure and Tensile Properties of P/M and I/M Al-Li-X Alloys.* Aluminum-Lithium Alloys, T. H. Sanders, Jr. and E. A. Starke, Jr., ed., TMS-AIME, Warrendale, PA, 1981, p. 263-291.
9. LIN, F. S., CHAKRABORTTY, S. B., and STARKE, Jr., E. A. *Microstructure-Property Relationships of Two Al-2Li-2Cu-0.2Zr-xCd Alloys.* Met. Trans. A., v. 13A, March 1982, p. 401-410.

In addition to the coarse 1.8-μm-diameter grain boundary precipitates, several finer precipitates were also present and were observed via TEM. Figure 6 is a superlattice dark field image of the 2090 matrix which revealed several second-phase precipitates. Readily observed precipitates included the spherical coherent δ' (Al_3Li) phase, the spherical composite δ'/β' (Al_3Zr) precipitate, and the T_1 (Al_2CuLi) and θ' (Al_2Cu) plates. Both T_1 and θ' plates were visible in the bright field image of Figure 7. A superlattice dark field image using a centered δ'/θ' reflection revealed brightly imaged δ' and θ' precipitates (see Figure 8). The δ' precipitates were 200 Å in diameter and precipitate-free zones were not observed along grain or subgrain boundaries.

SEM analyses of the fracture surfaces of two tensile specimens were performed to determine mode of fracture. The two tensile specimens were of different gauge diameter, one being 0.113 inch and the other 0.505 inch. As is standard practice for specimens of varying size, the crosshead speed of 0.05 in./min for the larger specimen was lowered to 0.005 in./min for the 0.113-inch specimen. The fracture surfaces of the tensile specimens revealed two different modes of fracture. The smaller tensile specimen exhibited a mixed ductile/intergranular fracture with microvoid coalescence around Al-Cu-Fe intermetallics (see Figure 9). Conversely, the large specimen fractured by a brittle transgranular cleavage mechanism (see Figure 10). Shear bands were evident (see Figure 11) as well as rods corresponding to the T_1 phase (see Figure 12).

Figure 6. Superlattice dark field image of 2090 matrix revealing δ', β'/δ', θ', and T_1 precipitates.

Figure 7. Bright field image showing T_1 and θ' plates.

Figure 8. Dark field image using δ'/θ' superlattice reflection.

Figure 9. SEM micrograph of tensile specimen tested at slow strain rate showing ductile/intergranular fracture.

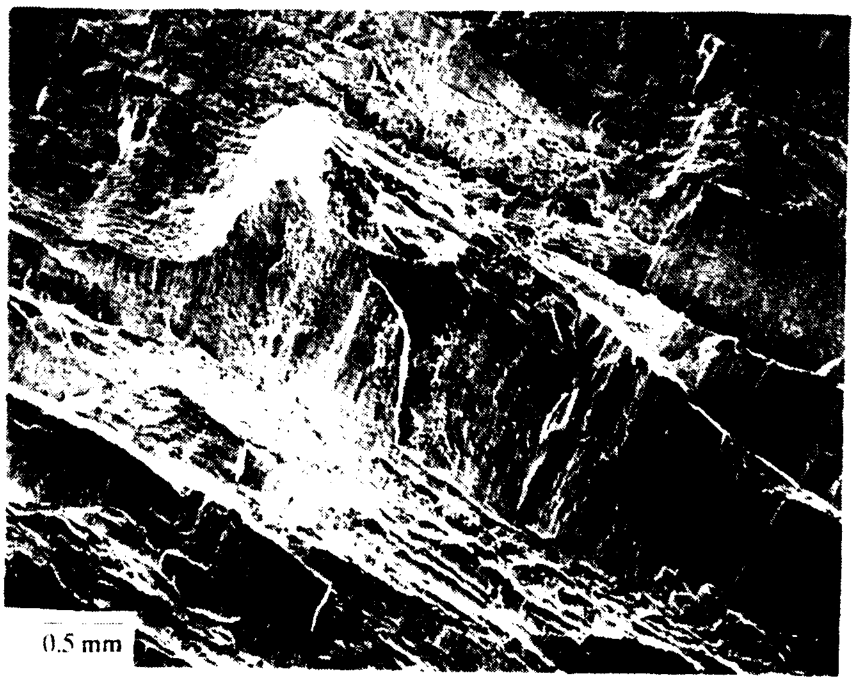

Figure 10. SEM micrograph of fracture surface of high strain rate tensile specimen indicating transgranular cleavage.

Figure 11. SEM micrograph of shear bands on fracture surface.

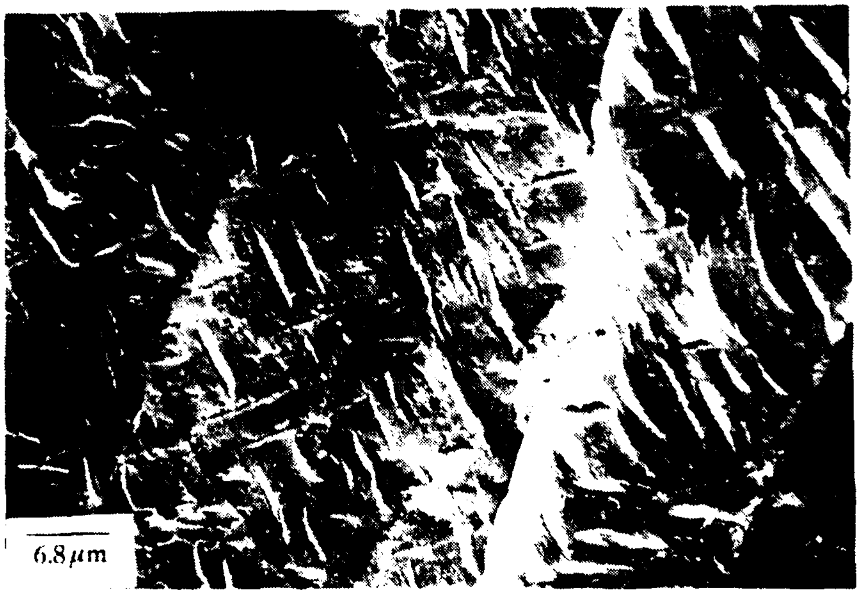

Figure 12. SEM micrograph of fracture surface of high strain rate tensile specimen revealing cleavage rods corresponding to T_1 phase.

The precipitates identified by TEM, primarily δ', T_1, and θ', are common to all Al-Li-Cu alloys.[10,11] These are the main strengthening precipitates. In addition, partially incoherent T_1 and θ' phases act to reduce the extent of strain localization compared to the binary Al-Li alloy.[9] Since the well-dispersed T_1 phase is anodic[12] with respect to the matrix, this would explain the pit nucleation observed throughout the specimen surface.

The coarse grain boundary precipitates observed corresponded to those identified in previous studies and were most likely a combination of Al_7Cu_2Fe and T_2 precipitates with some oxide phases also possible. The increased purity of the 2090-T8E48 plate resulted in grain boundaries which were less delineated with the Al_7Cu_2Fe and T_2 precipitates than those of the X2090-T8E41 plate. Fracture toughness values for the 2090-T8E48 and X2090-T8E41 plates were similar ($K_Q \approx 30$ ksi$\sqrt{\text{in.}}$), substantiating a previous conclusion that grain boundary precipitates had little or no effect on fracture path or fracture mode.[3] As was previously mentioned, crosshead speed during tensile testing was increased from 0.005 in./min for the 0.113-inch specimen to 0.05 in./min for the 0.505-inch specimen. This corresponded to an increased strain rate and resulted in a strength increase of 10 ksi. This indicated that the 2090-T8E48 alloy had a positive strain rate sensitivity[13] and that fracture mode was strain rate sensitive. The fracture mode transition observed between the low and high strain rate tensile specimens can be explained by this strain rate sensitivity. The 0.113-inch specimen, tested at the lower strain rate, fractured by a mixture of intergranular fracture along grain boundary precipitates and ductile void coalescence. The slower strain rate allowed nucleation of voids at the grain boundary precipitates and resulted in the ductile intergranular failure. The specimen tested at the higher strain rate failed by transgranular cleavage with higher strength and elongation. Transgranular cleavage or shear band failure at room temperature had been observed as the major failure mechanism in several studies of the Al-Li-Cu alloy.[14-16]

In summary, microstructural analysis of 2090-T8E48 revealed a cleaner alloy with less gross precipitations from impurities than X2090-T8E41. However, the results of this study have shown only slight mechanical property improvement in 2090-T8E48 over the previously tested X2090-T8E41. Furthermore, the problem with severe spall and delamination due to ballistic impacts still persisted.

CONCLUSIONS

1. Tensile and fracture toughness properties of 2090-T8E48 were only slightly better than properties of X2090-T8E41.

2. Mechanical property data agreed with ALCOA's data from limited testing.

3. Ballistic limit of 2090-T8E48 against cal. .30 AP M2 was slightly better than 2519-T87 and 7039-T67 aluminum armor alloys.

10. CASSADA, W. A., SHIFLET, G. J., and STARKE, Jr., E. A. *Electron Diffraction Studies of Al_2CuLi (T_1) Plates in an Al-2.4Li-2.4Cu-0.18Zr Alloy.* Scripta Met., v. 21, 1987, p. 387-392.
11. STARKE, Jr., E. A., and SANDERS, Jr., T. H. *New Approaches to Alloy Development in the Al-Li System.* Journal of Metals, August 1981, p. 24-32.
12. DORWARD, R. C., and HASSA, K. R. *Stress Corrosion Characteristics of AlCuLi 2090 Alloy.* Corrosion, v. 44, no. 13, December 1988, p. 932-941.
13. MEYERS, M. A., and CHAWLA, K. K. Mechanical Metallurgy Principles and Applications. Prentice-Hall, Englewood Cliffs, NJ, 1984.
14. JATA, K. V., and STARKE, Jr., E. A. *Fatigue Crack Growth and Fracture Toughness Behavior of Al-Li-Cu Alloy.* Aluminum Lithium Alloys III, C. Baker, P. J. Gregson, S. J. Harris, and C. J. Peel, ed., Institute of Metals, London, UK, 1986, p. 247-256.
15. HUANG, J. C., and ARDELL, A. J. *Microstructural Evolution in Two Al-Li-Cu Alloys.* Aluminum Lithium Alloys III, C. Baker, P. J. Gregson, S. J. Harris, and C. J. Peel, ed., Institute of Metals, London, UK, 1986, p. 453-470.
16. VENKATESWARA RAO, K. T., YU, W., and RITCHIE, R. O. *Cryogenic Toughness of Commercial Aluminum-Lithium Alloys: Role of Delamination Toughening.* Met. Trans. A., v. 20A, March 1989, p. 485-497.

4. Ballistic limit of 2090-T8E48 against 20-mm FSP was lower than 2519-T87 and 7039-T67.

5. Severe spalling and delamination from ballistic testing precluded 2090-T8E48 as an armor candidate.

6. The S-T and S-L orientation had K_{Iscc}'s of between 5 ksi$\sqrt{in.}$ to 7 ksi$\sqrt{in.}$.

7. The T-L orientations had a K_{Iscc} of 12 ksi$\sqrt{in.}$ to 13 ksi$\sqrt{in.}$.

8. There are large amounts of gel formation [$Al(OH)_3$ and LiOH] at all corrosion pits and cracks which retard SCC.

9. The 2090-T8E48 alloy has extremely poor pitting resistance. Furthermore, preferential pitting at any stress point was observed.

10. Fracture mode was not affected by coarse grain boundary precipitates but was found to be strain-rate sensitive. Brittle transgranular cleavage was the primary fracture mode.

DISTRIBUTION LIST

No. of Copies	To
1	Office of the Under Secretary of Defense for Research and Engineering, The Pentagon, Washington, DC 20301
	Commander, U.S. Army Laboratory Command, 2800 Powder Mill Road, Adelphi, MD 20783-1145
1	ATTN: AMSLC-IM-TL
1	AMSLC-CT
	Commander, Defense Technical Information Center, Cameron Station, Building 5, 5010 Duke Street, Alexandria, VA 22304-6145
2	ATTN: DTIC-FDAC
1	Metals and Ceramics Information Center, Battelle Columbus Laboratories, 505 King Avenue, Columbus, OH 43201
	Commander, Army Research Office, P.O. Box 12211, Research Triangle Park, NC 27709-2211
1	ATTN: Information Processing Office
	Commander, U.S. Army Materiel Command, 5001 Eisenhower Avenue, Alexandria, VA 22333
1	ATTN: AMCLD
	Commander, U.S. Army Materiel Systems Analysis Activity, Aberdeen Proving Ground, MD 21005
1	ATTN: AMXSY-MP, H. Cohen
	Commander, U.S. Army Missile Command, Redstone Scientific Information Center, Redstone Arsenal, AL 35898-5241
1	ATTN: AMSMI-RD-CS-R/Doc
1	AMSMI-RLM
	Commander, U.S. Army Armament, Munitions and Chemical Command, Dover, NJ 07801
2	ATTN: Technical Library
1	AMDAR-LCA, Mr. Harry E. Pebly, Jr., PLASTEC, Director
	Commander, U.S. Army Natick Research, Development and Engineering Center, Natick, MA 01760
1	ATTN: Technical Library
	Commander, U.S. Army Satellite Communications Agency, Fort Monmouth, NJ 07703
1	ATTN: Technical Document Center
	Commander, U.S. Army Tank-Automotive Command, Warren, MI 48397-5000
1	ATTN: AMSTA-ZSK
2	AMSTA-TSL, Technical Library
	Commander, White Sands Missile Range, NM 88002
1	ATTN: STEWS-WS-VT
	President, Airborne, Electronics and Special Warfare Board, Fort Bragg, NC 28307
1	ATTN: Library
	Director, U.S. Army Ballistic Research Laboratory, Aberdeen Proving Ground, MD 21005
1	ATTN: SLCBR-TSB-S (STINFO)
	Commander, Dugway Proving Ground, Dugway, UT 84022
1	ATTN: Technical Library, Technical Information Division
	Commander, Harry Diamond Laboratories, 2800 Powder Mill Road, Adelphi, MD 20783
1	ATTN: Technical Information Office
	Director, Benet Weapons Laboratory, LCWSL, USA AMCCOM, Watervliet, NY 12189
1	ATTN: AMSMC-LCB-TL
1	AMSMC-LCB-R
1	AMSMC-LCB-RM
1	AMSMC-LCB-RP
	Commander, U.S. Army Foreign Science and Technology Center, 220 7th Street, N.E., Charlottesville, VA 22901
1	ATTN: Military Tech

No. of Copies	To
	Commander, U.S. Army Aeromedical Research Unit, P.O. Box 577, Fort Rucker, AL 36360
1	ATTN: Technical Library
	Commander, U.S. Army Aviation Systems Command, Aviation Research and Technology Activity, Aviation Applied Technology Directorate, Fort Eustis, VA 23604-5577
1	ATTN: SAVDL-E-MOS
	U.S. Army Aviation Training Library, Fort Rucker, AL 36360
1	ATTN: Building 5906-5907
	Commander, U.S. Army Agency for Aviation Safety, Fort Rucker, AL 36362
1	ATTN: Technical Library
	Commander, USACDC Air Defense Agency, Fort Bliss, TX 79916
1	ATTN: Technical Library
	Commander, U.S. Army Engineer School, Fort Belvoir, VA 22060
1	ATTN: Library
	Commander, U.S. Army Engineer Waterways Experiment Station, P. O. Box 631, Vicksburg, MS 39180
1	ATTN: Research Center Library
	Commandant, U.S. Army Quartermaster School, Fort Lee, VA 23801
1	ATTN: Quartermaster School Library
	Naval Research Laboratory, Washington, DC 20375
1	ATTN: Code 5830
2	Dr. G. R. Yoder - Code 6384
	Chief of Naval Research, Arlington, VA 22217
1	ATTN: Code 471
1	Edward J. Morrissey, AFWAL/MLTE, Wright-Patterson Air Force, Base, OH 45433
	Commander, U.S. Air Force Wright Aeronautical Laboratories, Wright-Patterson Air Force Base, OH 45433
1	ATTN: AFWAL/MLC
1	AFWAL/MLLP, M. Forney, Jr.
1	AFWAL/MLBC, Mr. Stanley Schulman
	National Aeronautics and Space Administration, Marshall Space Flight Center, Huntsville, AL 35812
1	ATTN: R. J. Schwinghammer, EH01, Dir, M&P Lab
1	Mr. W. A. Wilson, EH41, Bldg. 4612
	U.S. Department of Commerce, National Institute of Standards and Technology, Gaithersburg, MD 20899
1	ATTN: Stephen M. Hsu, Chief, Ceramics Division, Institute for Materials Science and Engineering
1	Committee on Marine Structures, Marine Board, National Research Council, 2101 Constitution Ave., N.W., Washington, DC 20418
1	Librarian, Materials Sciences Corporation, Guynedd Plaza 11, Bethlehem Pike, Spring House, PA 19477
1	The Charles Stark Draper Laboratory, 68 Albany Street, Cambridge, MA 02139
	Wyman-Gordon Company, Worcester, MA 01601
1	ATTN: Technical Library
	Lockheed-Georgia Company, 86 South Cobb Drive, Marietta, GA 30063
1	ATTN: Materials and Processes Engineering Dept. 71-11, Zone 54
	General Dynamics, Convair Aerospace Division, P.O. Box 748, Fort Worth, TX 76101
1	ATTN: Mfg. Engineering Technical Library
1	Mechanical Properties Data Center, Belfour Stulen Inc., 13917 W. Bay Shore Drive, Traverse City, MI 49684
	Director, U.S. Army Materials Technology Laboratory, Watertown, MA 02172-0001
2	ATTN: SLCMT-TML
4	Author

U.S. Army Materials Technology Laboratory
Watertown, Massachusetts 02172-0001
EVALUATION OF 2090-T8E48
ALUMINUM-LITHIUM PLATES -
Ernest S. C. Chin, Marietta R. Cappucci,
Robert M. Huie, and Robert E. Pasternak

Technical Report MTL TR 89-97, November 1989, 19 pp-
illus-tables, D/A Project: 1L162105.AH84

AD______________
UNCLASSIFIED
UNLIMITED DISTRIBUTION

Key Words

Aluminum alloys
Lithium alloys
Tensile strength

A 1.5-inch-thick 2090-T8E48 aluminum-lithium (Al-Li) alloy plate was evaluated in conjunction with the Navy Cooperative Test Program. Mechanical characterization included testing of tensile specimens in the longitudinal, transverse, and short direction, and testing of compact tension/slow bend specimens covering the L-T, T-L, L-S, S-L, S-T, and T-S directions. In addition, ballistic tolerance against caliber .30 armor piercing projectile and 20-mm fragment simulated projectile was determined. Corrosion and stress corrosion studies were made in accordance with ASTM standards. Microstructural characterization was performed through optical metallography and transmission electron microscopy. Consolidation and discussion of all the results in comparison with previously evaluated 0.5-inch-thick X2090-T8 is presented.

U.S. Army Materials Technology Laboratory
Watertown, Massachusetts 02172-0001
EVALUATION OF 2090-T8E48
ALUMINUM-LITHIUM PLATES -
Ernest S. C. Chin, Marietta R. Cappucci,
Robert M. Huie, and Robert E. Pasternak

Technical Report MTL TR 89-97, November 1989, 19 pp-
illus-tables, D/A Project: 1L162105.AH84

AD______________
UNCLASSIFIED
UNLIMITED DISTRIBUTION

Key Words

Aluminum alloys
Lithium alloys
Tensile strength

A 1.5-inch-thick 2090-T8E48 aluminum-lithium (Al-Li) alloy plate was evaluated in conjunction with the Navy Cooperative Test Program. Mechanical characterization included testing of tensile specimens in the longitudinal, transverse, and short direction, and testing of compact tension/slow bend specimens covering the L-T, T-L, L-S, S-L, S-T, and T-S directions. In addition, ballistic tolerance against caliber .30 armor piercing projectile and 20-mm fragment simulated projectile was determined. Corrosion and stress corrosion studies were made in accordance with ASTM standards. Microstructural characterization was performed through optical metallography and transmission electron microscopy. Consolidation and discussion of all the results in comparison with previously evaluated 0.5-inch-thick X2090-T8 is presented.

U.S. Army Materials Technology Laboratory
Watertown, Massachusetts 02172-0001
EVALUATION OF 2090-T8E48
ALUMINUM-LITHIUM PLATES -
Ernest S. C. Chin, Marietta R. Cappucci,
Robert M. Huie, and Robert E. Pasternak

Technical Report MTL TR 89-97, November 1989, 19 pp-
illus-tables, D/A Project: 1L162105.AH84

AD______________
UNCLASSIFIED
UNLIMITED DISTRIBUTION

Key Words

Aluminum alloys
Lithium alloys
Tensile strength

A 1.5-inch-thick 2090-T8E48 aluminum-lithium (Al-Li) alloy plate was evaluated in conjunction with the Navy Cooperative Test Program. Mechanical characterization included testing of tensile specimens in the longitudinal, transverse, and short direction, and testing of compact tension/slow bend specimens covering the L-T, T-L, L-S, S-L, S-T, and T-S directions. In addition, ballistic tolerance against caliber .30 armor piercing projectile and 20-mm fragment simulated projectile was determined. Corrosion and stress corrosion studies were made in accordance with ASTM standards. Microstructural characterization was performed through optical metallography and transmission electron microscopy. Consolidation and discussion of all the results in comparison with previously evaluated 0.5-inch-thick X2090-T8 is presented.

U.S. Army Materials Technology Laboratory
Watertown, Massachusetts 02172-0001
EVALUATION OF 2090-T8E48
ALUMINUM-LITHIUM PLATES -
Ernest S. C. Chin, Marietta R. Cappucci,
Robert M. Huie, and Robert E. Pasternak

Technical Report MTL TR 89-97, November 1989, 19 pp-
illus-tables, D/A Project: 1L162105.AH84

AD______________
UNCLASSIFIED
UNLIMITED DISTRIBUTION

Key Words

Aluminum alloys
Lithium alloys
Tensile strength

A 1.5-inch-thick 2090-T8E48 aluminum-lithium (Al-Li) alloy plate was evaluated in conjunction with the Navy Cooperative Test Program. Mechanical characterization included testing of tensile specimens in the longitudinal, transverse, and short direction, and testing of compact tension/slow bend specimens covering the L-T, T-L, L-S, S-L, S-T, and T-S directions. In addition, ballistic tolerance against caliber .30 armor piercing projectile and 20-mm fragment simulated projectile was determined. Corrosion and stress corrosion studies were made in accordance with ASTM standards. Microstructural characterization was performed through optical metallography and transmission electron microscopy. Consolidation and discussion of all the results in comparison with previously evaluated 0.5-inch-thick X2090-T8 is presented.